Unsteady Phenomena during Transient Process in Radial Vanelss Diffuser

Nobutaka HAYASHI[1], Tomohiko TAGAWA[2], Masaharu KOYAMA[1], Icihro ARIGA[1],
and Masatoshi SANO[1]

[1]Department of Mechanical Engineering
Chiba Institute of Technology
2-17-1 Tsudanuma, Narashino-shi, Chiba, 275-0016, Japan
Phone: +81-47-478-0269 FAX: +81-47-478-0299, E-mail: p01koyam@ｐｆ.ｉｔ-ｃｈｉｂａ.ａｃ.ｊｐ

[2] T-TEC Co., Ltd

ABSTRACT

In centrifugal compressors, diffusers are some of the main components for the pressure recovery function, and they play an important role in the performance of compressors. Generally, as flow rate reduces, compressors have a limited operation range due to rotating stall. This paper describes the unsteady process during the generation of rotating stall in a radial vaneless diffuser. The wall static pressure was measured using pressure transducer attached on the diffuser wall. The acquired data was analyzed using various DSP methods.

INTRODUCTION

As the flow rate reduces, self-exciting phenomena such as surge and rotating stall that lead to damage of the machine occur in the centrifugal vaneless diffuser. In comparison to surge, rotating stall generally occurs at a higher flow rate; thus, when the compressor is at low flow rate, the operating range is limited by the generation of rotating stall. If rotating stall can be controlled, the operating range of compressors can be expanded. For this reason, researchers are engaged in a variety of studies. For example, Tsurusaki et al.(1986) and Watanabe and Ariga(1993) provided detailed measurements of velocity in vaneless diffuser during rotating stall. Through such studies, the aspects of the flow field during rotating stall are nearly clarified.

On the other hand, the generation process of rotating stall is not elucidated. The aforementioned Watanabe and Ariga (1993) found that weak, periodic fluctuation occurred intermittently static pressure fluctuation signal of diffuser wall in the transient process leading to the onset of rotating stall. Also, Lawless and Fleeter (1995) have reported on the behavior of rotating stall after performing continuous FFT analyses of signals measured while gradually throttling the flow rate and utilizing high-sensitivity microphones attached to the diffuser wall. However, the results of such research are based on information obtained from the vicinity of the diffuser inlet and do not mention how the static pressure fluctuation accompanying rotating stall is propagated in the diffuser radial direction. The flow field inside the diffuser is known to be complex as reverse flow regions are alternately produced on the shroud side and hub side, even in flow region where rotating stall does not occur (Watanabe and Ariga,1993, Senoo et al.,1977). It is still not clear as to how rotating stall is generated and develops in such complex flow field.

In order to investigate the transient process that leads to rotating stall from the viewpoint of static pressure field, multiple-point simultaneous measurements of the wall static pressure were taken using pressure transducers attached to the diffuser wall and as the flow rate was continuously changed. By performing continuous FFT analysis, wavelet analysis, and other signal processing for obtained data, the authors tried to illuminate rotating stall onset and transitional development process.

EXPERIMENT AND MEASUREMENT METHOD

The experiment was conducted using an axially symmetric vaneless diffuser installed on the downstream of an open-loop centrifugal blower as shown in Figure 1. Incidentally, the dimensions of the major components are also shown in Figure 1. The suction nozzle was installed at the apparatus inlet. The flow rate was measured by the pressure transducer at the inlet of the suction nozzle. The impeller revolution was maintained at 2000 rpm by inverter control. The flow rate was adjusted with a butterfly valve installed downstream from the nozzle inlet. The diffuser had a width b of 0.017 m and an outside diameter of 0.862 m. The impeller had an outside diameter of 0.345 m and outlet width of 0.017 m, while using fifteen backswept blades oriented at an outlet angle of 45°. Also, the Reynolds number (Re) for the diffuser inlet (= ub/v; u: impeller tip speed; v: kinematic viscosity) was 4.1×10^4.

The pressure measurement made use of a semiconductor diffusion-type pressure transducers (Toyoda PD 104 KW, resonant frequency of 6 kHz) that was attached on the diffuser shroud side. At that time, signals from the pressure transducer were sampled at 1 ms by an A/D converter via a 20 Hz low-pass filter in order to

① Inlet nozzle
② Flow control valve
③ Pulse motor
④ Straightener
⑤ Impeller
⑥ Vaneless Diffuser
L1 : 0.5m, L2 : 0.925m
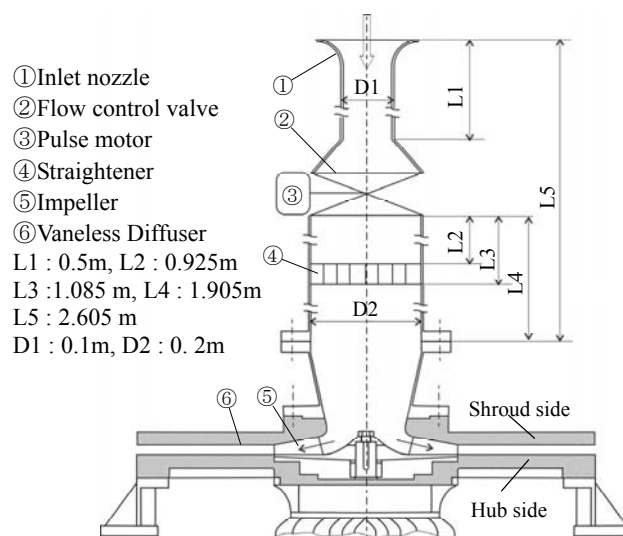L3 :1.085 m, L4 : 1.905m
L5 : 2.605 m
D1 : 0.1m, D2 : 0. 2m

Fig.1 Experimental apparatus

eliminate the effects of the noise due to impeller's rotation. As shown in Figure 2, five lines containing ten measurement holes were made on the shroud side within the range $r_i/r_0 = 1.1$ to 2.0 (r_i: position of static pressure hole on diffuser wall; r_0: impeller radius). The diameter of these holes was 0.8 mm, and pressure transducers were connected to the end. Since multiple-point simultaneous measurements were performed using multiple pressure transducers, these transducers were attached carefully to ensure uniformity at all measurement points. And as a preliminary experiment, the pressure transducers were calibrated and the frequency characteristics were confirmed. The frequency characteristics of these transducers were confirmed up to 500 Hz which is rotational frequency of impeller.
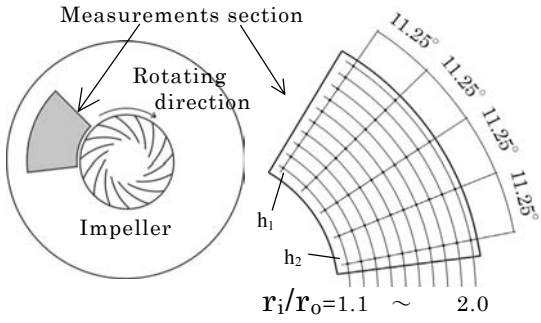

Fig.2 Schema of shroud side of the diffuser

RESULTS AND DISCUSSION

Diffuser Performance

Figure 3 shows the relationships of the pressure recovery coefficient, C_p and flow coefficient, ϕ, which are defined in Eq. (1) and Eq. (2).

$$C_p = \frac{P_2 - P_1}{\rho u^2 / 2} \quad (1)$$

$$\phi = \frac{Q}{Au} \quad (2)$$

P_1 : Static pressure at diffuser wall (ri/r0 = 1.1)

P_2 : Static pressure at diffuser wall (ri/r0 = 2.0)

Q : Corrected flow rate

A : Area of impeller outlet
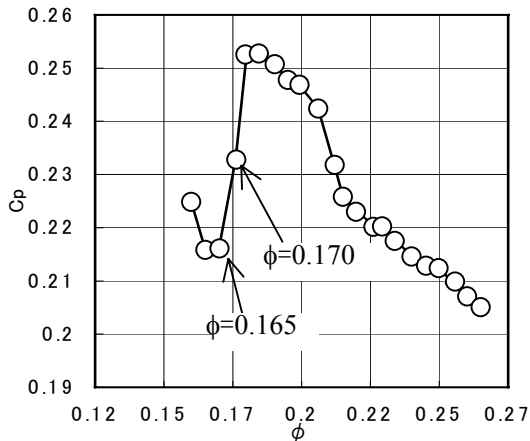
u : Impeller tip speed

ρ : Air density

Fig.3 Performance curve

From Figure 3, it is clear that the pressure recovery coefficient, C_p, increases as the flow coefficient ϕ decreases, but the diffuser performance rapidly drops at $\phi = 0.175$.

Figures 4(a) and (b) show the static pressure fluctuation signals at $\phi = 0.170$ and $\phi = 0.165$, measured at $r_i/r_0 = 1.1$. Figures 5(a) and (b) show the results of the corresponding FFT analyses. $\Delta t'$ in Figure 4 is the fluctuation period, while the vertical axis in Figure 5 is the pressure amplitude spectrum. From Figures 4 and 5, it is clear that as the diffuser's performance rapidly drops, periodic static pressure fluctuation occurs from $\phi = 0.170$ and that the frequency changes at $\phi = 0.165$. The waveform at $\phi = 0.170$ is a 4.7 Hz sinusoidal. The frequency changes at $\phi = 0.165$, becoming synthetic wave of 4.16, 8.33, 12.5, and 16.66 Hz.

In order to investigate how these periodic fluctuations are transmitted circumferentially, cross-correlation coefficients were calculated for the static pressure fluctuation signals at two points h_1 and h_2 mutually separated by 45° at $r_i/r_0 = 1.1$ (Figure 2); then the time lag Δt for the fluctuation at point h_2 with respect to the fluctuation at point h_1 was found. The results are shown in Figures 6(a) and (b). At $\phi = 0.170$, $\Delta t = 0.05$ s; while at $\phi = 0.165$, $\Delta t = 0.029$ s. Regardless of the flow coefficient, there is a positive time lag for the fluctuation at point h_2 with respect to the fluctuation at point h_1; moreover, it is clear that these fluctuations are propagated in the direction of the impeller's rotation. Next, the number of cells was calculated, using Eq. (3) based on these time lags (Fringe and Braembussche, 1983, Wachter and Rieder,1985).
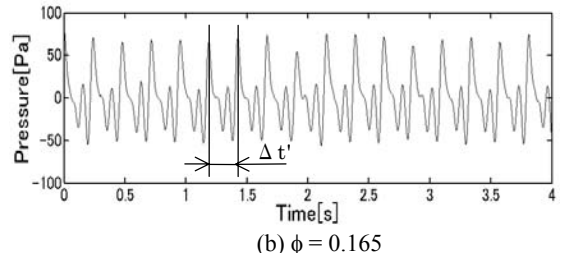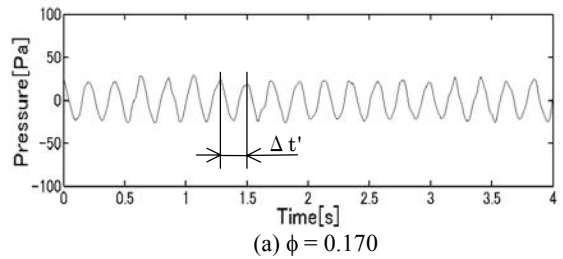

(a) $\phi = 0.170$

(b) $\phi = 0.165$

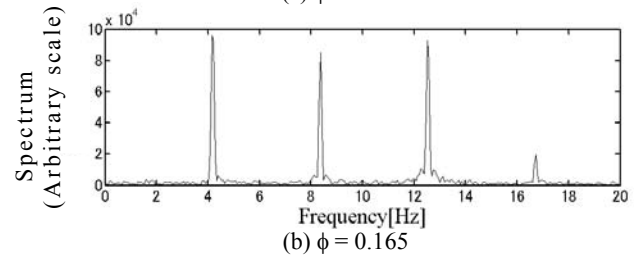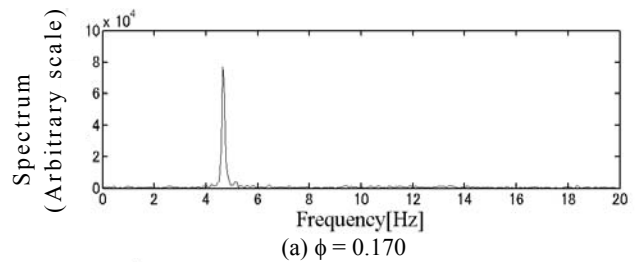Fig.4 Pressure signal at $r_i/r_0=1.1$

(a) $\phi = 0.170$

(b) $\phi = 0.165$

Fig.5 FFT analysis

To find the fluctuation period Δt' shown in Figure 4, the results of the FFT analysis in Figure 5 were used. At ϕ = 0.170, Δt' = 1/4.7 s; while at ϕ = 0.165, Δt' = 1/4.16 s, the reciprocal of the lowest frequency.

$$Number\ of\ cells = \frac{\Delta t \times 360}{45} \times \frac{1}{\Delta t'} \quad (3)$$

Δt : Time lag of two fluctuations
Δt' : Fluctuation period

Consequently, rotating stall with two cells occurred at ϕ = 0.170, and one cell at ϕ = 0.165. Decreasing the flow rate, waveform of the static pressure fluctuation signal at the onset of rotating stall becomes sinusoidal. As the flow rate is further throttled, this condition shifts to rotating stall characterized by a synthetic-wave-type static pressure fluctuation. This same condition has been reported by other researchers as well (Watanabe and Ariga, 1993, Abdelhamid et al., 1978). Watanabe and Ariga(1993) also reported that the number of cells change from 2 to 1. However, there have been only a few reports that have investigated in detail the transient process between the two types of rotating stalls.
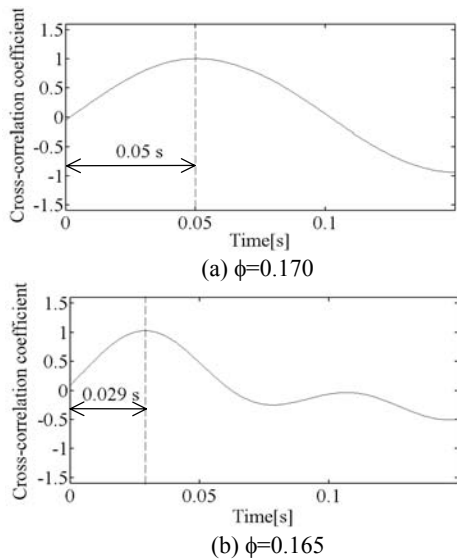

(a) ϕ=0.170

(b) ϕ=0.165

Fig.6 Cross-correlation coefficient

Rotating Stall Onset and Transient Process
In order to investigate in detail the transition process from the stable region to the region in which the two types of rotating stall occur, the flow rate was decreased by gradually throttling the valve controlled by pulse motor and the static pressure was measured between ϕ = 0.174 and 0.163, where the performance rapidly drops. Measurements were taken at two points, r_i/r_0 = 1.1 and 2.0, along the same radius. Since similar signal appeared at both locations, the signal at r_i/r_0 = 1.1 was used as the reference example as shown in Figure 7, in which the flow coefficients at the time t=0, 28.84, 56.97 and 70 s, respectively, are indicated. Figure 7(a) shows the signal from 0 to 70s, (b) shows the expanded signal in the vicinity of ϕ = 0.170, and (c) shows the expanded signal in the vicinity of ϕ = 0.165. As shown in Figure 7, the signal can be divided into three regions; A is the region over ϕ = 0.170 where the signal is random form, B is from ϕ = 0.170 to ϕ = 0.165 where the signal is sinusoidal wave, and C is under ϕ = 0.165 where the signal is synthetic wave of a few frequencies.

Figure 8 shows the results of a continuous FFT analysis that was conducted with the signal of Figure 7(a) multiplying Hanning window. From Figure 8, it is clear that weak pressure fluctuations with approximately 4 and 10 Hz occur in region A, a peak of approximately 4 Hz grows up in region B, and peaks of approximately 4, 8, 12, and 16 Hz sharply grow up in region C. Abdelhamid et al.(1978) reported on the gradual change in signal that occurs in the transition from region A to region B. However, there have been no detailed reports on how the frequency changes.

Next, from the data for the fluctuations at r_i/r_0 = 1.1 and 2.0, the cross-correlation coefficients were calculated and it was investigated how the pressure fluctuation propagates in radial direction. The results are shown in Figure 9. The horizontal axis, as with the continuous FFT analysis, represents the time from the start of throttling; while the vertical axis represents the time lag of the two fluctuations (time lag of the fluctuation at r_i/r_0 = 1.1 with respect to the fluctuation at r_i/r_0 = 2.0). The black-and-white patterns shows contours for the correlation coefficients. From these results, too, it is clear that the correlation coefficient distribution changes and can be divided into three regions at the same time periods as in Figure 7. As the flow rate drops and moves into region B from ϕ = 0.170, the correlation coefficient peak abruptly changes at a positive position where the time lag is near 0.02 s. As the flow rate becomes lower and region transits to region C, the time lag gets smaller. In region C under ϕ = 0.165, the time lag abruptly approaches 0 s, and it can be seen that the fluctuation reaches the entire diffuser. On the other hand, the trends of region B and C are not seen in region A.
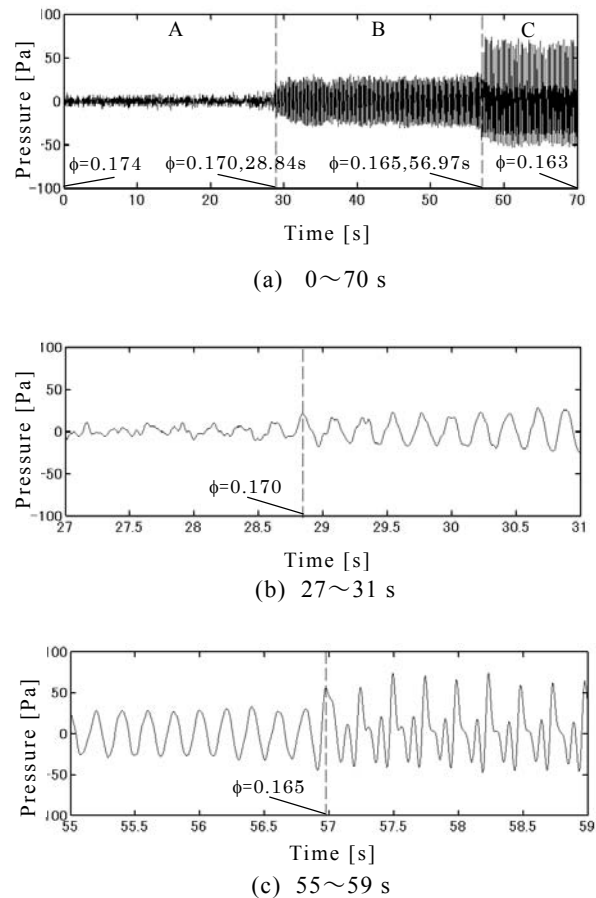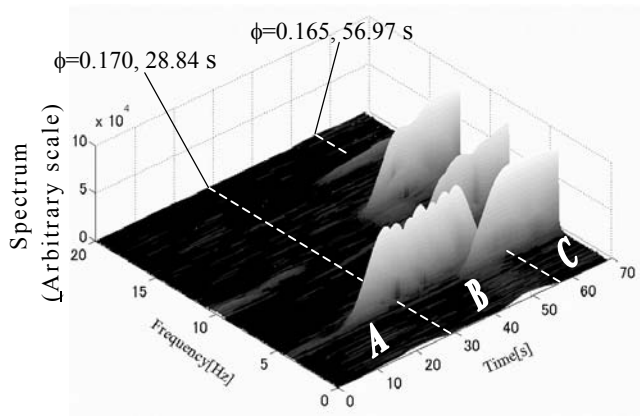

(a) 0～70 s

(b) 27～31 s

(c) 55～59 s

Fig.7 Pressure signal at r_i/r_0=1.1

Fig.8 Continuous FFT analysis
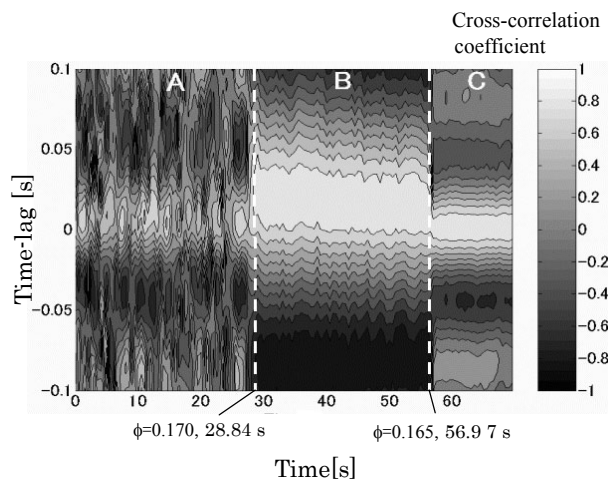

Fig.9 Cross-correlation contour

Fig.10   Pressure distribution at φ=0.170

In order to examine the phenomena of region B and C from a different viewpoint, the wall static pressure was measured during the occurrence of 2 types of rotating stall at fifty measurement holes on the shroud side.

The pressure fluctuations were measured with six pressure transducers. The phases of each signal were brought into line after data sampling, based on the signal at measurement hole h_1. The contours of Figures 10 and 11 are the results of these data ensemble averaged in the rotating stall period. Each figure is the wall static pressure distribution at the pressure signal peak at measurement hole h_1, and shows the change in the stall region that occurs during a single rotation of a stall cell.

At φ = 0.170, a high-pressure region appears downstream from the diffuser at each positive peak of the reference signal in Figures 10 (a) thru (e). It is clear from the instants shown in Figures 11 (a) and (e) that at φ = 0.165 the high-pressure area has entered further upstream. Since these high pressure region appears at the peaks of the reference signal, it is thought that the periodic pressure fluctuations that occur during rotating stall are produced when this area rotates at a certain speed. Although this has also been pointed out by Watanabe and Ariga (1993), the study described here confirmed the penetration of these high pressure region into the diffuser's upstream area at lower flow rate. This result backs up the results of analysis using cross-correlation coefficients, namely, that the static pressure fluctuation propagates from the diffuser downstream.
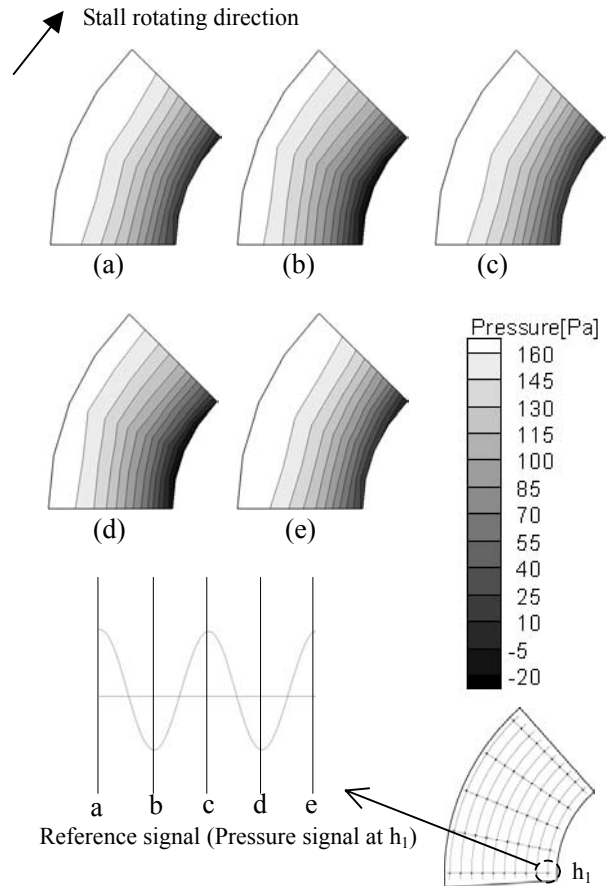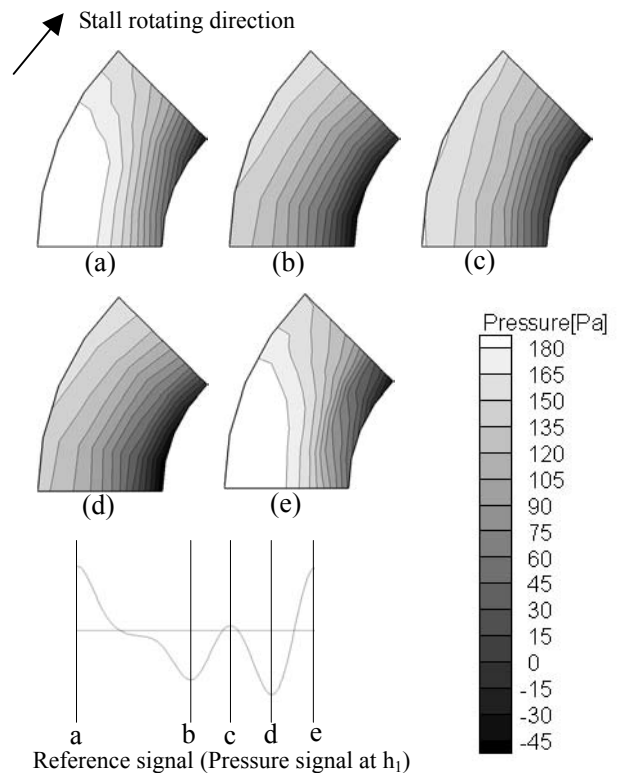

Fig.11 Pressure distribution at φ=0.165

Wavelet Analysis

At a glance the signal in region A of Figure 7 dose not appear to have regularity. But from the results of the continuous FFT analysis in Figure 8, it is clear that fluctuations of approximately 4 and 10 Hz occur weakly. This indicates that periodic pressure fluctuations are continuously occurring in region A. Also, Figures 7 and 8 showed that the rapid change occurs from the sinusoidal waveform in region B to the synthetic waveform in region C. Thus, using FFT analysis, it is difficult to gain an understanding of such phenomena in which the frequency intermittently or rapidly changes with time. For this reason, wavelet analysis was conducted.

In recent years, wavelet analysis has been used in various fields. For example, in the field of fluid dynamics, research has been conducted on the behavior of Karman vortex formed in the wake of a circular cylinder (Ishikawa et al., 1995). It is also used in research on the rotating stall of a axial compressor in the field of turbo machinery (Inoue et al., 1999). However, there are very few examples in which wavelet analysis has been used to analyze in detail the onset and transient process of rotating stall occurring in centrifugal vaneless diffusers. Continuous wavelet transform is a method of calculating the correlation of mother wavelet with targeted signals while changing the shift parameter of the mother wavelet defined in Eq. (4), as well as the scale parameter corresponding to the frequency. The scale parameter corresponds to the reciprocal of the frequency. By having the vertical axis represent the scale parameter, and the horizontal axis the time, we can understand the relationship between the time and frequency.

$$W(a,b) = \int \frac{1}{\sqrt{a}} \psi^* \left(\frac{t-b}{a} \right) f(t) dt \quad (4)$$

$W(a,b)$: Wavelet coefficient

$\psi^*(t)$: Mother wavelet(conjugate)

$f(t)$: Signal

a : Scale parameter

b : Shift parameter

With wavelet analysis, the targeted frequency range will vary according to the mother wavelet selected. In this study Morlet wavelet as shown in Eq. (5) was adopted. To decompose the signal as referred in later section, only the real part was used. As coefficient k, k=5 was used. Although various number can be taken as coefficient k, k=5 is often selected in practice (Daubechies, 1992). The compatibility of the utilized mother wavelet was confirmed by actually analyzing test signal that combined sine waves at the target frequencies of 4 and 10 Hz. Also, calculations were performed using a scale from 1 to 500, changing at increments of 1.

$$\psi(t) = exp\left(\sqrt{-1}k \cdot t \right) exp\left(-\frac{t^2}{2} \right) \qquad (5)$$

Figures 12 and 13 show the results of continuous wavelet transform performed for the signals in Figure 7. Figures 12 and 13 are wavelet coefficient isograms. Incidentally, the frequency on the vertical axis is the frequency of each scale's mother wavelet. Moreover, the upper signal is the analyzed pressure signal. During the analysis, the 25-30 s range of signal in Figure 7 was used as shown in Figure 12, and the 55.5-58.5 s range of signal in Figure 7 was used as shown in Figure 13, in which the transition to a signal having rotating stall of two cells, as well as the transition to rotating stall from two cells to one cell, is shown.

As shown in Figure 12, the fluctuation near 4 Hz gradually weakens, while a fluctuation near 10 Hz grows up from about 25.5 s. In Figure 8, it appears as if the fluctuations occurring near 4 and
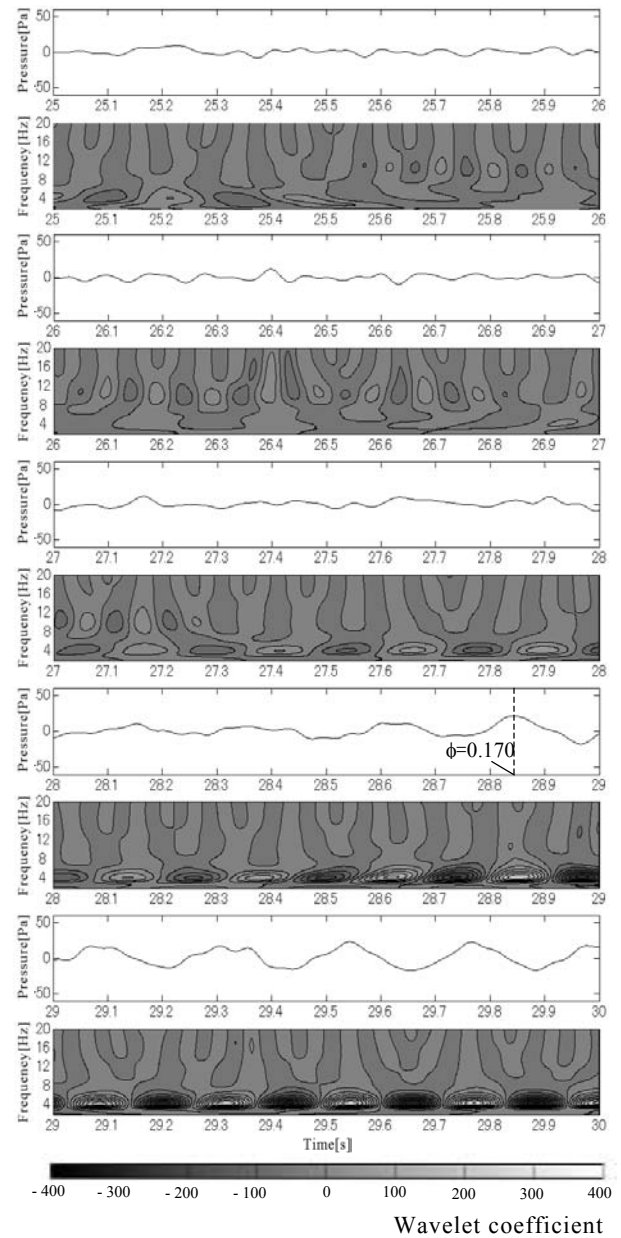

Fig.12 Continuous wavelet analysis (25～30s)

10Hz in entire region A. In fact, they occur intermittently. Also, as the fluctuations near 10 Hz weaken from about 26.9 s, the fluctuations near 4 Hz become remarkably strong. And from about 28.84 s at $\phi = 0.170$, a complete rotating stall of two cells occurs. As mentioned in the introduction, it has been reported by Watanabe and Ariga (1993) that precursor signs referred to as prestall occurs intermittently before the onset of rotating stall. That report states that wall static pressure fluctuations corresponding to the rotating stall of two cells occur intermittently during low flow rate, that the fluctuations become continuous when the flow rate becomes even lower, and that ultimately there is a transition to a fluctuation corresponding to the rotating stall of one cell. As mentioned previously, it is clear that wall static pressure fluctuation caused by rotating stall occur as reported by Watanabe and Ariga (1993). Since the fluctuations near 4Hz which occur at 25 to 25.5s before the onset of rotating stall correspond to the frequency of rotating stall of two cells, this fluctuation is thought to be prestall. Also, as the wall static pressure fluctuations near 10 Hz dissipate, the fluctuations near 4 Hz become evident; thus, the dissipation of the fluctuations near 10 Hz is also thought to be a type of precursor of rotating stall. Then as the condition shifts toward an even lower

flow rate, there is a transition to rotating stall of one cell at 56.97 s, where $\phi = 0.165$ in Figure 13. This transition is abrupt, and it is clear that there will be no precursor such as the prestall that occurs during the onset of rotating stall.
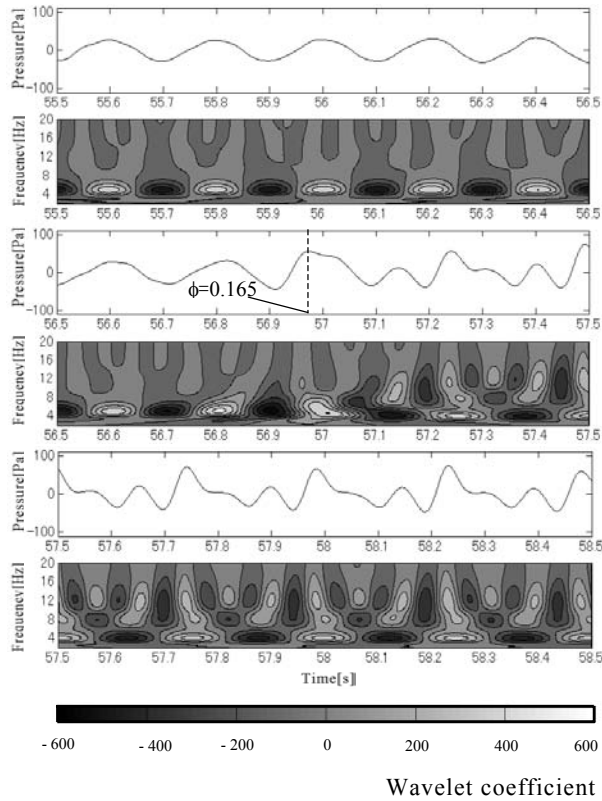

Fig.13 Continuous wavelet analysis (55.5～58.5s)

Propagation of pressure fluctuation at onset of rotating stall
    Next, the authors investigated how the static pressure fluctuations near 4 Hz were propagated in radial direction at the onset of rotating stall of two cells. While continuously throttling the flow rate from $\phi = 0.171$ to $\phi = 0.170$ at which the rotating stall of two cells starts, the wall static pressure was measured simultaneously at seven points on the same radius at $r_i/r_0 = 1.1$ to 1.7. The signals were decompose with continuous wavelet transform. The signals shown in Figures 14 and 15 are the pressure signal at $r_i/r_0 = 1.1$ and the extracted signal of 4.2 Hz which correspond to the frequency of rotating stall of two cells at $r_i/r_0 = 1.1$. In both Figures 14 and 15, 0 s is the time at $\phi = 0.171$, while 6 s is the time at $\phi = 0.170$. The same process was used for each radius ratio. The extracted signals were divided into 4 parts as shown in Figure 15 by positive peak times of the signal at $r_i/r_0 = 1.1$. Using cross-correlation, the authors calculated the timelag of the extracted signal with each radius ratio at 4 timing (time lag of the fluctuation at $r_i/r_0 = 1.1$ with respect to the fluctuation of each radius ratio). The results are shown in Figure 16, where the vertical axis represents the time lag, and the horizontal axis the radius ratio. Figure 16 clearly shows the propagation of the fluctuation occurring at the diffuser outlet propagates to diffuser inlet. If the fluctuation propagates at a fixed propagation velocity from the diffuser downstream to the upstream, the time lag is expected to change linearly in the radial direction. But in Figure 16, it is clear that the form is nonlinear. In ① and ②, the time lag gets smaller in a nearly uniform manner from $r_i/r_0 = 1.7$ to $r_i/r_0 = 1.3$, then gets larger at $r_i/r_0 = 1.2$ before becoming at zero at $r_i/r_0 = 1.1$. From these results, it is thought that the wall static pressure fluctuation that was produced

at $r_i/r_0 = 1.7$ in ① and ② does not reach the diffuser inlet. But from ③ and thereafter, it can be assumed that when the time lag at $r_i/r_0 = 1.2$ becomes larger than at $r_i/r_0 = 1.3$, the wall static pressure fluctuation propagates to the diffuser inlet from $r_i/r_0 = 1.7$. Also the propagation varies according to the radius ratio. Based on the slope of the curves in Figure 16, the curves in ③ and thereafter (where the rotating stall is developed) can be divided into three ranges: at $r_i/r_0 = 1.1$-1.2, 1.2-1.5, and 1.5-1.7. If the slope in Figure 16 corresponds to the radial propagation velocity, the propagation velocity of the fluctuation propagated from $r_i/r_0 = 1.7$ increases for a time at $r_i/r_0 = 1.5$-1.2, then decreases again at $r_i/r_0 = 1.2$-1.1.
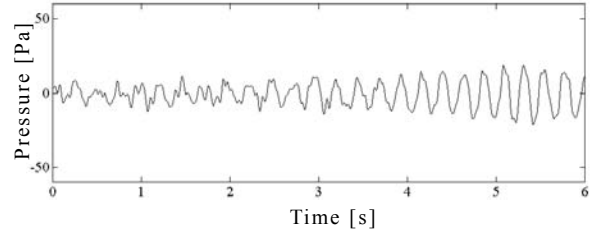

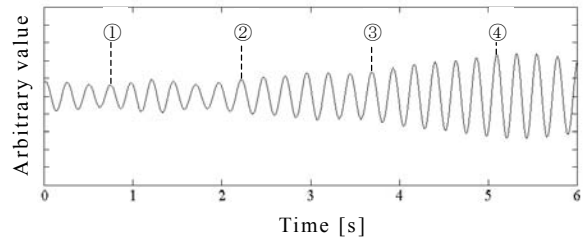Fig.14   Raw signal at $r_i/r_o = 1.1$

Fig.15 Extracted signal and peak location (4.2 Hz)
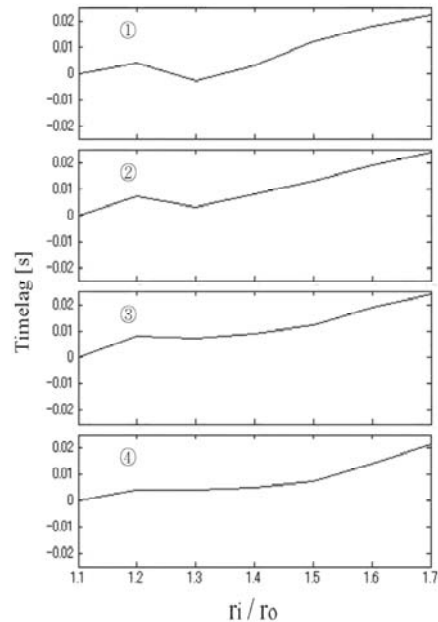

Fig.16 Spatial distribution of time lag

CONCLUSION

In this study, multiple-point simultaneous measurements of the wall static pressure were taken, using pressure transducers installed on the shroud walls of a centrifugal vaneless diffuser testing rig. The following conclusions were obtained:

(1) The diffuser performance rapidly drops and rotating stall of two cells occurs as the flow rate decreases. As the flow rate becomes lower, the condition shifts to rotating stall of one cell.

(2) Static pressure fluctuations accompanying rotating stall of two cells propagates from the diffuser downstream to the upstream, and static pressure fluctuations accompanying rotating stall of one cell further penetrates into the diffuser inlet.

(3) From the results of continuous wavelet analysis, it became clear that a static pressure fluctuation corresponding to the frequency of rotating stall of two cells and approximately twice frequency of rotating stall of two cells occur before the onset of rotating stall. It also became clear that as the aforementioned higher-frequency static pressure fluctuation dissipates, rotating stall of two cells starts.

(4) Before the onset of rotating stall, a static pressure fluctuation occurs at the diffuser downstream region at a frequency equivalent to rotating stall of two cells.

(5) The propagation velocity of a static pressure fluctuation that is propagated in the diffuser radial direction at the onset of rotating stall will vary according to the radius ratio.

REFERENCES

Tsurusaki, H., Imaichi, K., and Miyake, R., 1986, "A Study on the Rotating Stall in Vaneless Diffusers of Centrifugal Fans," *Trans. JSME*, Vol. 52, No. 480, pp. 2930-2938.

Watanabe, H., Ariga, I., 1993, "Transient Process of Rotating Stall in Radial Vaneless Diffuser," *Trans. JSME*, Vol. 59, No. 565, pp. 2848-2854.

Lawless, P. B. , and Fleeter, S., 1995, "Rotating Stall Acoustic Signature in a Low-Speed Centrifugal Compressor: Part 1-Vaneless Diffuser," *ASME, J. Turbomach*, Vol. 117, pp.87-96.

Senoo, Y., Kinoshita, Y., and Ishida, M., 1977, "Asymmetric Flow in Vaneless Diffusers of Centrifugal Blowers," *Trans. ASME Journal of Fluids Eng*. Vol. 99, No. 1, pp. 104-114.

Fringe, P., and Van Den Braembussche, R., 1983, "Distinction Between Different Types of Impeller and Diffuser Rotating Stall in a Centrifugal Compressor With Vaneless Diffuser," *ASME, Paper*, 83-GT-61.

Wachter, J., Rieder, M ., 1985, "Influence of Design Data on the Onset and Behavior of Rotating Stall in a Single Centrifugal Compressor," *VDI, Berichte*, 572, pp.591-605.

Abdelhamid, A. N., Colwill, W. H., and Barrows, J. F., 1978, "Experimental Investigation of Unsteady Phenomena in Vaneless Radial Diffusers," *ASME, Paper,* 78-GT-23.

Ishikawa, H., Kiya, M., and Mochizuki, O., 1995, "Analysis of a Turbulent Wake by the Wavelet Transform," *Trans. JSME*, Vol. 61, No. 587, pp. 2409-2417.

Inoue, M., Kuroumaru, M., Tanino, T., Maeda, S., and Furukawa, M., 1999, "Development of Multiple Cells with Short Length-Scale Stall in an Axial Compressor Rotor," *Trans. JSME*, Vol. 65, No. 640, pp. 4021-4026.

Daubechies, I., 1992, "Ten Lectures on Wavelets," pp76, SIAM.